JCTC Journal of Chemical Theory and Computation

Article

pubs.acs.org/JCTC

Insights on P-Glycoprotein's Efflux Mechanism Obtained by Molecular Dynamics Simulations

Ricardo J. Ferreira, Maria-José U. Ferreira, and Daniel J. V. A. dos Santos*

Research Institute for Medicine and Pharmaceutical Sciences (iMed.UL), Faculty of Pharmacy, University of Lisbon, Av. Prof. Gama Pinto, 1649-003 Lisbon, Portugal

Supporting Information

ABSTRACT: P-Glycoprotein (P-gp) is often involved in multidrug resistance (MDR) to the pharmacological action of a wide number of anticancer agents. In this article, a series of molecular dynamics simulations of murine's P-gp were developed, elucidating the importance of the lipid membrane and linker sequence in the protein structure stability. The behavior of several molecules inside the drug-binding pocket revealed a striking difference between substrates or modulators, and motion patterns were identified that could be correlated with conformational alterations due to substrate binding, corresponding to the initial step in the efflux mechanism. Only one "entrance gate" to the drug-binding pocket was found and, in the presence of a substrate, leads to changes in the motion patterns of the transporter into an efflux-like movement.

P-Glycoprotein (P-gp) is the most representative member of the ABC transporter proteins superfamily, often implicated in the multidrug-resistance phenomenon (MDR).[1,2] This transporter expels a wide-range of substrates out of the cell (mainly hydrophobic) through an ATP-dependent mechanism.[2,3] It has a molecular weight of ∼170 kDa organized in two functional units with pseudo-2-fold molecular symmetry, each one comprising six transmembranar α-helices domains (TMD) and one cytoplasmic nucleotide-binding domain (NBD), linked by a small polypeptidic sequence.[4]

There is still great controversy about the efflux mechanism of this type of transporter. The first studies claimed that the extrusion of the molecules can occur directly from the cytoplasmic compartment[5] or that the protein could act according to a flippase model.[6] More recently, the hydrophobic vacuum-cleaner model[7] became the most accepted theory, supported by several studies that correlate the diffusion of the transported molecules within the inner leaflet of the cellular membrane with interactions at the drug-binding site (DBS).[3,8]

The large majority of the most recent studies accept an alternate cycle for the ATP hydrolysis,[9,10] emphasizing the fact that only transported substrates at the DBS, in conjunction with ATP binding, can induce conformational changes in the protein structure leading to the extrusion of the molecule.[11] As a direct consequence, the energy driven from ATP hydrolysis must be used to reset the transporter into its original conformation, thus allowing new catalytic cycles.[10] However, the communication routes between DBS-NBD and the extent of the conformational changes leading to the efflux mechanism are still mainly unknown. In addition, the lipidic composition[12−14] and global passive permeation rate of molecules through the plasmatic membrane[15,16] also seem to be as important as the transporter itself, working together as a single entity rather than two distinct structures.[17,18]

The crystallization of membrane proteins is proved to be difficult, greatly diminishing the number of available structures in the Protein Data Bank (PDB). Nevertheless, these proteins are of great importance due to their physiological functions as neurotransmitter receptors, ion channels, or, in the case of P-gp, ATP-driven substrate transporters. In particular, the crystallographic structure of such transporters can be used as a framework to allow a better comprehension of their mechanism of action. For instance, the crystallographic information obtained from BtuCD, a vitamin B12 importer, suggested the existence of communication between drug-binding and nucleotide-binding sites as a way to induce the catalytic cycle, possibly triggered by long-range conformational changes developed by the binding and/or hydrolysis of ATP.[19]

Recently, a murine P-glycoprotein crystallographic structure was made available in the PDB[20,21] (ID: 3G5U) with a 3.8 Å resolution.[22] This information made possible the identification of one large internal chamber of approximately 6000 Å^3—the drug-binding pocket (DBP)—delimited by the TMD but opened to the intracellular compartment and the inner leaflet of the membrane through two "gates" formed by the pairs TMD 4/6 and 10/12.[22] Inside the binding pocket, 73 exposed residues were identified, of which 15 are polar and only two charged or possibly charged (His60 and Glu871). Three drug-binding sites were proposed based on the chemical characteristics of the amino acids present in each one and on docked structures with the inhibitors QZ59-RRR and QZ59-SSS. Therefore, this study refers to the possible simultaneous binding of two compounds inside the DBP.[22] Several studies also propose that the internal cavity may be filled with water molecules and that 70% of the area attributed to the DBS is due to the transmembranar domains 3, 5, 6, 8, 11, and 12, also implying TMD 6 and 12 in the translocation process.[23,24]

In the meantime, the lack of a crystallographic structure led to the development of several homology models for ABC transporters mainly derived from bacterial templates such as Sav1866,[25,26] MalK,[27] or MsbA.[28] Although later proved

Received: February 1, 2012
Published: May 9, 2012

inaccurate as prediction models[29,30] largely due to errors introduced during the homology process, it was possible to obtain relevant information related with the ABC transporters primary function. These models, obtained from *apo* structures (open,[27,28] semiopen,[27] or closed[28] conformational states) or in the presence of nucleotides (AMP-PNP,[28,31] ADP,[32] and ADP-Vi[28]), were employed in later studies that suggested the rigid-body rotation of the NBD as the major driving force for the induction of TMD reorganizations and NBD dimerization. The TMD reorganization is indeed supported by studies which claim that the rotation of the helices into an asymmetric conformational state can be the major event that alters the affinity of the DBS,[10,33,34] leading to the ejection of the molecule from the internal cavity to the outside of the cell. More recent computational studies have also characterized the magnitude of such conformational alterations in stages after and before ATP hydrolysis,[35] in NBD dimerization,[36] and following the removal of ATP/Mg^{2+},[37] confirming the pivotal role of TMD6 in the efflux mechanism.[37] These observations are of great value for the analysis of the P-gp translocation mechanism, due to the similarity between the structures.

The murine crystallographic structure has also been recently used as a framework for an increasing number of docking studies.[38,39] Such studies are important because they can provide useful information about the intrinsic molecular properties that discriminate molecules like verapamil[40] or tariquidar,[41] known P-gp inhibitors, from substrates like vinblastine[40] or colchicine.[1] However, the presence of water molecules inside the DBS can be a major drawback in this type of study, usually made in the absence of water. In addition, the published crystallographic structure was obtained in the absence of a lipid bilayer membrane and is incomplete, lacking the information correspondent to the structure of a linker region between the Ala627 and Ala683, located about half-way into the P-gp sequence. This region and its flexibility were proved to be important for the regulation of the substrates' specificity toward human P-gp, also interfering with the conformational change that accompanies the hydrolysis of the ATP molecule.[42,43]

Despite all evidence, a clear demonstration of the transporter normal modes of motion is still missing, along with the clarification of the NBD dimerization and helix rotation as the principal motion pattern associated with the efflux mechanism. In this particular case, computational investigations can be valuable tools for the identification of such patterns. Computational models have been used for the simulation of biological systems in order to further understand the data obtained through previous studies, thus enlightening the biological process mechanism of action, substrate binding or conformational alterations. More specifically, the application of the molecular dynamics (MD) technique to P-gp models can unveil some answers regarding the structure's stability, drug-binding locations, translocation processes, and interactions with the surrounding lipid bilayer. From such techniques, normal-mode analysis and functional mode analysis of the protein movements are important tools, allowing the comparison between simulations of the *apo* and *holo* structures, with one or several molecules inside the DBP. All of the above methods could lead to the identification of the movements intimately related with the translocation process, aiming for a better understanding of the first steps of the efflux mechanism.

In this paper, we describe a series of P-gp computational MD simulations based on the murine crystallographic data. The objectives are as follows:

i. to refine and validate a P-gp structure, suitable for utilization in later studies; the missing linker sequence and lipid bilayer membrane will be assessed, in order to evaluate the importance of such structures in the stabilization of the protein
ii. to evaluate the behavior of several molecules (substrates or inhibitors), inside the DBP, by analyzing the type and number of contacts established and major residues involved in the ligand−protein interactions
iii. to assess modifications in the normal motion patterns displayed by the transporter, in order to identify conformational changes that can be associated with the efflux mechanism, when perturbed by a molecule suitable to be transported

MATERIAL AND METHODS

Initial Structures and Software. The murine P-glycoprotein structure (ID: 3G5U) was obtained from the Protein Data Bank (www.pdb.org)[20] and parametrized according to the GROMOS96[44,45] force field with the 53a6[46] parameter set. Two lipid bilayers (dimiristoyl-phosphatidylcholine—DMPC—and 1-palmitoyl-2-oleoylphosphatidylcholine—POPC) and respective parametrization were obtained from previous simulations by Poger et al.[47,48] This choice of lipid parametrization took into account the ability to correctly reproduce properties of lipid bilayers,[49] namely, the area and volume per lipid ratios[47,50,51] and fluid-phase[47,48,52,53] or solvation[47,48,53] properties.

Protein manipulation, protonation, and linker modeling were made in MOE 2009.10.[54] The GROMACS simulation packages, 4.5.x,[55−57] were used for the MD simulations and later bilayer constructions. The *InflateGRO*[58] script was initially employed in bilayer builds and later substituted by the *g_membed*[59] module available in the GROMACS package. The *GridMAT-MD*[60] script was used to calculate areas per lipid (A_L) of the protein-bilayer systems. Functional mode analysis (FMA) was done as described by Hub and de Groot,[61] covariance analysis[62] with auxiliary programs available in GROMACS, and principal component analysis (PCA) performed using the ProDy[63,64] software. Substrates and inhibitors parametrization were prepared online using the PRODRG[65] or the Automated Topology Builder and Repository[66] servers, and Mülliken partial charges were assigned through ab initio calculations at the Hartree−Fock level of theory using the 6-31G(d) basis set in the Gaussian 03[67] program. VMD[68] and MOE were used for molecular inspection and visualization.

Systems Construction. *Initial Evaluation.* The crystallographic P-gp structure was solvated (41 664 water molecules) and the system's total charge neutralized with the addition of 25 chlorine atoms (SOL-I). After energy minimization, a 1 ns *NVT* equilibration run was performed (spatially restraining the protein's heavy atoms) followed by a 10 ns *NPT* unrestricted run. Another system was built comprising the crystallographic P-gp inserted into a 417 lipid DMPC membrane (DMPC-I), water soaked (57 628 molecules) and neutralized (with an adequate number of counterions). The position of the membrane relative to P-gp was defined using information obtained from the OPM database.[69] The system was energy minimized and equilibrated with two sequential *NVT* (1 ns) and *NPT* (10 ns) runs, spatially restraining the protein's heavy atoms.

Finally, an unrestricted *NPT* run was performed, with a duration of 30 ns.

Linker. The folding of the missing linker was assessed through secondary structure prediction online servers such as NetSurfP,[70] APSSP,[71] PROF,[72] and CFSSP.[73] The segment was then built with the Protein Builder module of MOE, followed by protonation and energy minimization. The distance between the amine and carboxyl groups of terminal residues was kept to the crystallographic length of the linker (4.75 Å). The resulting structure was then solvated (with the correct number of counterions added) and further equilibrated in GROMACS through a series of eight MD simulations (*NVT*), each one at 500 ps duration and with different initial parameters (temperature, thermostat, and/or interaction cutoff radius) in order to obtain different starting points for the runs. An *NPT* run for each one of the eight linker structures followed for 4 ns using the same simulation parameters. Using these run data, all obtained structures were then evaluated regarding the system's final energies, a Ramachandran[74] plot for structural stability and visual evaluation. The more suitable conformation was then added to the whole protein with the protonation status of the entire protein evaluated once more through MOE's *Protonate3D* module.

Construction of the Membrane Systems. The correct relative position of the lipid bilayer was defined according to the OPM database[69] information. After membrane insertion, the system was solvated and neutralized with an adequate number of chloride ions. A 20 ns equilibration run followed by restraining all heavy atoms of the P-gp crystallographic structure but three residues directly connected to each side of the linker, in order to allow a better adjustment between this segment and the entire structure. The resulting P-gp structure inserted into a POPC bilayer was the starting point for the structure refinement step.

Refinement Protocol. The whole P-gp structure was inserted into a previously equilibrated POPC membrane, water soaked (55 909 molecules), and neutralized with 26 chlorine ions, originating a system with 204 227 atoms. The system was energy minimized and a 100 ps *NVT* equilibration run followed, above the phospholipids gel-fluid transition phase,[75] at 303 K. Using the final structure of this run, two systems were obtained by applying two equilibration protocols. In the first (POPC-I), the initial 3 ns were made with heavy-atom spatial restraints, thus allowing the correct adjustment between the protein structure and the surrounding lipids. A 100 ns production run followed. On the second (POPC-II), the spatial restriction of the protein's heavy atoms was progressively removed, through a series of three successive *NPT* simulations of 500 ps each. The first one restrained heavy atoms from the mainchain (allowing the equilibration of the residue side chains to the lipid environment). The second restrained the backbone, and finally, the third restrained the α-carbons. The resulting system was used in a 100 ns production run.

Insertion of Ligands. For the systems with ligands inside the DBP, six molecules (inhibitors—verapamil,[40] tariquidar,[41] latilagascene E,[76] QZ59-SSS[22]—and substrates—colchicine,[1] vinblastine;[1,40] chemical structures available in Table S1 of Supporting Information) were positioned inside the internal cavity described by Aller et al. in three different positions, thus obtaining 18 new systems. After minimization, the systems were allowed to equilibrate for 1 ns, keeping the protein heavy atoms' positions restrained, after which three 20 ns production runs were performed (no restrictions applied). The two runs containing the largest molecules (vinblastine and tariquidar) in the top position of the DBP were later extended to 40 ns. Protein−ligand contacts were evaluated at every 250 ps to calculate the type, nature, and maximum number of established interactions using the LIGPLOT[77] software, in conjunction with HBPLUS.[78]

An additional system containing a vinblastine molecule at the entrance gate was also built. The molecule was inserted using a docking protocol available in MOE by performing 10 runs of simulated annealing, each comprising six cycles and defining an iteration limit of 4000 at an initial temperature of 1000 K, after which the best ranked pose was chosen. The resulting system was treated under the conditions above-described for the ligands inside the DBP.

Simulation Parameters. In all simulations, periodic boundary conditions (PBC) were applied. Simple energy minimizations were performed using the steepest descent method. All *NVT* runs used a Velocity-rescale (V-rescale) thermostat.[79] *NPT* runs used the Nosé−Hoover[80,81] thermostat and the Parrinello−Rahman[82,83] barostat for temperature (303 K) and pressure coupling (1 bar), respectively. In the presence of membranes, the pressure equilibration was achieved through a semi-isotropic pressure coupling. The system compressibility was defined as 4.5×10^{-5} bar^{-1}, and the initial box was defined with dimensions *xyz* of $12.75 \times 12.75 \times 16.55$ nm. The Particle Mesh Ewald (PME) method with cubic interpolation,[84,85] with an identical cutoff radius for electrostatic and van der Waals interactions (12 Å), was employed. The SETTLE[86] (for water molecules) or LINCS[87] algorithms were used to constrain all bond lengths.

RESULTS

P-gp Structure Refinement. As an initial evaluation of the crystallographic structure stability, a 10 ns simulation without a lipid bilayer was performed (SOL-I), revealing increased TMD disorganization and NBD separation leading to an irreversible distortion of the structure. This clearly shows the importance of the linker sequence and of the lipid bilayer. Therefore, the protein was inserted into membranes comprising different lipids (DMPC or POPC) in order to minimize the principal structural abnormalities observed.

The insertion of the protein, without the linker sequence, in each membrane type revealed a striking difference. It is known that the optimum insertion angle for the P-gp in a lipid membrane has a value of approximately 4°,[69] but in the DMPC membrane simulation (DMPC-I) this value rose to approximately 18° after 10 ns, while in a POPC membrane the insertion angle did not suffer significant alterations from the initial insertion angle. This difference between both systems can be explained by the difference between the thickness of the hydrophobic core of the simulated POPC (3.27 ± 0.03 nm) and DMPC membranes (2.85 ± 0.06 nm) against the 3.18 ± 0.12 nm[69] estimated for the P-gp (hydrophobic mismatch of 3.3 Å for DMPC). Therefore, in a system containing a DMPC bilayer, a tilting is expected to occur to maximize the contact area between hydrophobic regions of the P-gp and the lipids.[87] Additionally, eukaryotic membranes are richer in polyunsaturated lipids than saturated ones, a fact by which the POPC lipid is more adequate for the simulation of such transporters, in agreement with a previous study on a similar framework.[88]

In order to assess the importance of the linker in the stability of the whole structure, the corresponding secondary structure was built on the basis of secondary structure prediction

programs. A more exhaustive characterization was also made at PredictProtein.org,[89] which confirmed that 87.72% of the residues were exposed and the probability for the occurrence of structures as α-helix or β-sheets was only 10.53%. This is corroborated by the initial equilibration, with implicit solvent, in MOE (Figure 1). Sequences that favor protein−protein

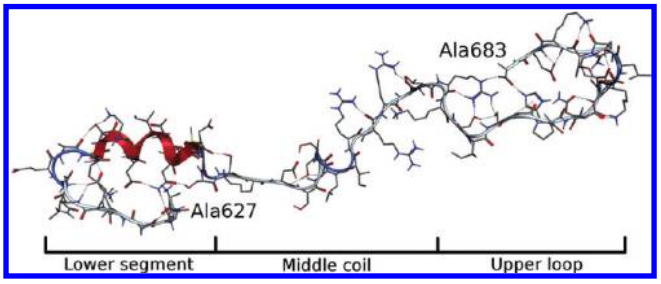

Figure 1. Predicted linker secondary structure showing the α-helix segment, the C-terminal Ala683, and N-terminal Ala627 residues.

interactions (Met-Leu-Asp and Lys-Ser-Ile) were identified, with a sequence with the ability to interact with nucleotides (Arg-Ser-Thr-Arg-Lys) also being recognized. The predicted secondary structure did not suffer major alterations during the subsequent equilibration process, even when inserted into P-gp and in the presence of a lipid bilayer. However, some fluctuations in the size of the helix and the formation of a small β-sheet in the middle coil have been registered during the POPC-II simulation.

The addition of the linker structure to the whole protein had a strong positive effect on the stability of the transporter. In the DMPC-I system, the initial tilt angle of P-gp remained unaffected this time, with the hydrophobic mismatch being instead compensated by an increase in the total thickness of the membrane. In the systems containing POPC lipids, the insertion of the linker greatly decreases the fluctuations and the distance variations between the two NBD domains. This is mainly due to the greater flexibility observed in this particular linker structure that acts as an intermediary between the two NBDs, thus increasing the stability of the intracellular portion of the protein (Chart 1). These findings support the fact that the presence of the linker sequence and the membrane are, indeed, essential to the stabilization of the whole structure. Since the crystallization of the protein was made in the absence of ATP, we chose to equilibrate the structure in the *apo* form as a way to evaluate the stability of the structure and simultaneously to clarify the influence of the missing linker and the lipid bilayer. As observed, and since the addition of these two structures had a significant impact on the transporter, the influence of the ATP molecule should be better studied using a refined structure.

A production run (POPC-I) was then performed, and after 100 ns, it was observed that severe distortions occurred in the protein's transmembranar helices (mainly TMD6 and 12) with direct influence on the packing of both NBDs, particularly noticeable in the disorganization of the NBD outer helices (data not shown). The crystallographic structure has relatively low resolution (3.8 Å), frequently implying the existence of main-chain and/or side-chain errors, namely in the rotamers.[90,91] As such, a series of consecutive runs with milder equilibration conditions were applied to a new system (POPC-II) as a way to reduce the impact of the low resolution in the final structure quality. In this simulation, the structure stabilization occurs

Chart 1. Root Mean Square Fluctuations (RMSF) of the α-Carbon for the P-gp Domains, in the Absence (black) or Presence of Linker (red), on a POPC Membrane[a]

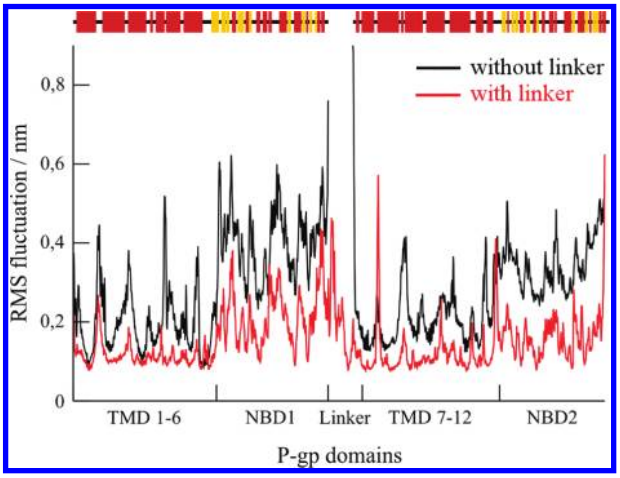

[a]A scheme of the secondary structure is displayed at the top, with α-helices in red and β-sheets in yellow.

more rapidly (within the first 10 ns), and the distortion of the structure is reduced. This milder equilibration protocol allows a better adjustment between the residues' side-chains and the surrounding lipid environment. All of the subsequent structure refinement data report to the POPC-II simulation.

The comparison between Ramachandran plots of the initial crystallographic structure and at the end of 100 ns shows a substantial reduction of outlier residues in the structure (Chart 2). Most of the residues moved to more favorable positions, an increased organization in the β-sheet region and a reduction of the residues in the allowed positions of the Ramachandran plot being observed. All of the remaining outlier residues are located in coils (Figure 2), the only exceptions being Ser333 (TMD6) and Asn969 (TMD12).

In the structure obtained at the end of the POPC-II simulation, it is possible to see the linker loop located near the interface of the bilayer's inner leaflet (Figure 2), severely limiting the access to the internal cavity from the cytoplasm. The position of this upper loop is constant throughout the simulations, thus not validating the membranar pore as a model for the mechanism of action in this type of transporter.

The presence of the linker also contributes to the more effective stabilization of the NBD in the transporter, allowing the formation of a variable number of stable linker-NBD2 hydrogen bonds, namely, between Asp646-His1229 and Asp649-Ser1068/Ser1069/Gly1070.

The root-mean-square deviation (RMSD) gives quantitative information about the structure deviation from a reference, usually the structure used at the beginning of the run. When this parameter is plotted for each P-gp domain separately (Chart 3), it is clear that the linker greatly contributes to the total RMSD, a fact that is in agreement with a previous study showing that the flexibility of this segment is important in ATP hydrolysis and drug transport,[42] thus the difficulty for the determination of this particular segment through crystallography.

In addition, the decomposition of the linker's RMSD in three distinct segments (Figure 1) also gives valuable information about its behavior.

While the lower segment, packed between the two NBDs, shows on average the smaller RMSD value, the middle coil

Chart 2. Ramachandran Plots of the Initial Crystallographic Structure (left) and at the End of 100 ns Production Run (right)[a]

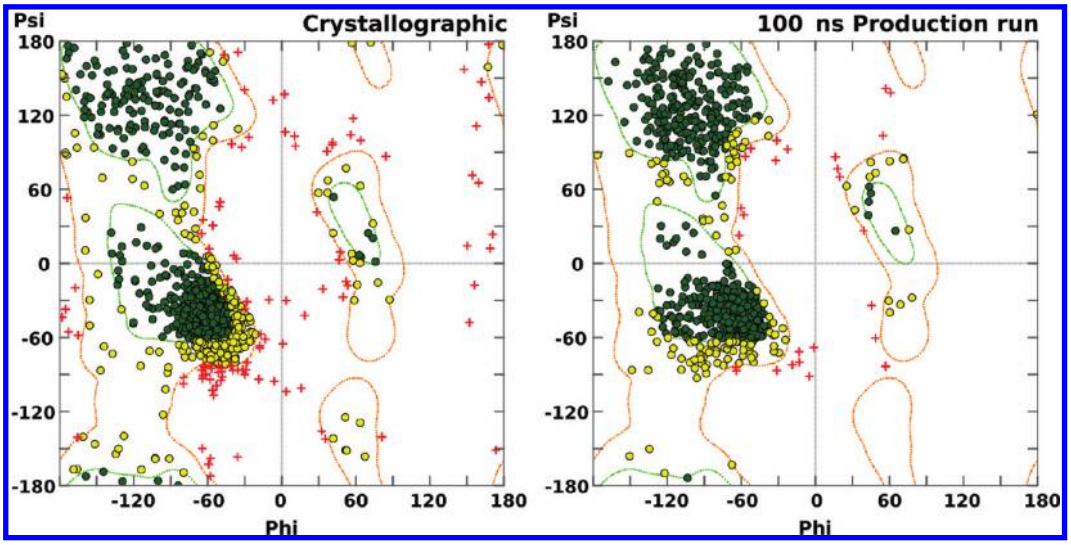

[a]Allowed regions are delimited by an orange curve and favored positions by a green curve.

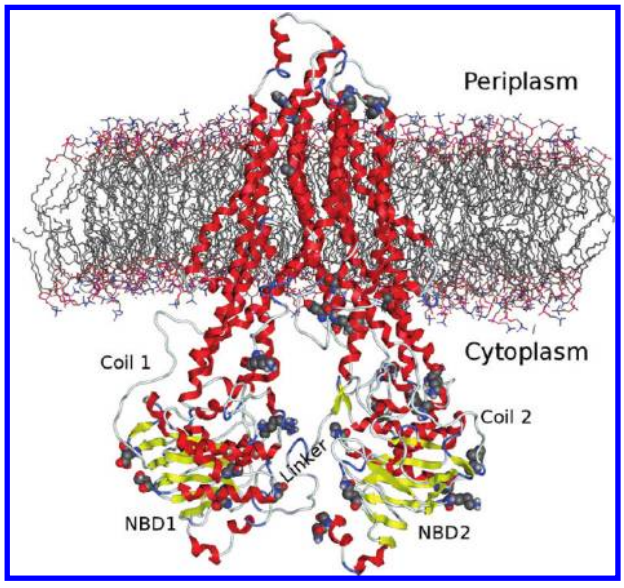

Figure 2. Final structure, with space-fill representation of the residues in unfavorable positions on the Ramachandran plot.

Chart 3. RMSD of Residue α-Carbons Grouped by Domains

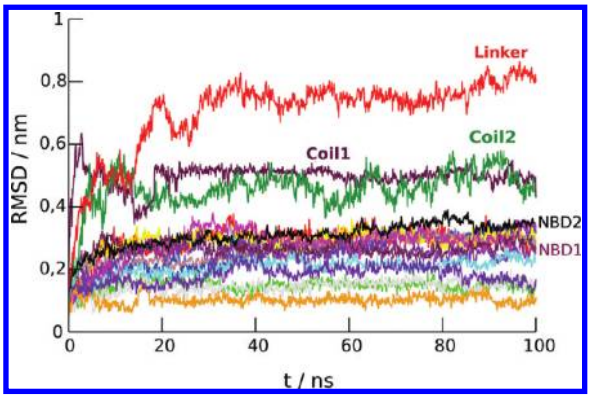

displays fluctuations through all of the simulation (Chart 4). For the upper loop, and despite the larger RMSD obtained, the

Chart 4. RMSD for the Linker, Plotted for Three Identified Sections in the Structure

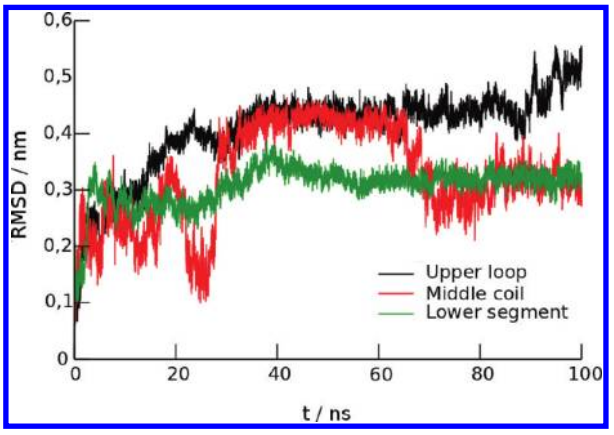

values registered are relatively constant after 30 ns. This fact can be related with an increased stability in the relative position of the upper loop, near the inner leaflet interface.

Chart 3 shows clearly that the remaining structure (helices and NBD) remains stable, within a maximum RMSD of about 3 Å, with the two coils connecting TMD6 to NBD1 (coil 1) and TMD12 to NBD2 (coil 2) presenting two of the largest RMSDs, well separated from the RMSD of the TMD and NBD. The P-gp domains that have the lowest RMSDs are helices 3 (light green), 7 (light gray), 8 (purple), and 11 (orange), within a maximum of 2 Å.

In this study, a prominent difference in the behavior of the portals assumed as gate entrances to the internal cavity from the inner leaflet was identified. Some studies suggest that the access to the DBS is possible through two portals, often identified between TMD 2/11 and 5/8[92] or, based on the crystallographic structure, between 4/6 and 10/12,[22] accessible only from the lipid bilayer. The low resolution of the murine crystallographic structure is unsuitable to provide a more definitive answer. Moreover, the absence of the linker does not allow a clear definition of the portals' lower boundaries. However, the data obtained from the POPC-II simulation show a different behavior between both portals: only the portal formed by TMD 10/12

dx.doi.org/10.1021/ct300083m | J. Chem. Theory Comput. 2012, 8, 1853−1864

gives access to the internal DBP from the inner leaflet core, with the 4/6 portal closed during all of the simulation.

The different behavior between the portals is also observable from the distance variations between the TMD. While the distance and the angle between TMD 4/6 tends to decrease, thus narrowing the gap and allowing the side-chains to effectively block the space in between (Figure 3, left), the gap between 10/12 and the angle between the helices remains relatively unchanged, allowing the formation of a channel to the interior of the cavity (Figure 3, right). These observations corroborate the hydrophobic vacuum-cleaner model, the permeation of the molecule into the inner leaflet being essential in order to gain access to the drug binding pocket and, this way, showing the importance of an adequate balance between the molecule's hydrophobic and hydrophilic properties. However, since we have not tested the full impact, combined or not, of ATP and substrates, we cannot speculate if the difference between TMD6 and TMD12 is maintained during the full efflux cycle. It is possible that TMD6 can move in order to open the gate in a later stage or, considering the alternate model[3] (in which ATP hydrolysis occurs alternately in NBD1 and NBD2), in a different step of the efflux mechanism. Moreover, a comprehensive study of the full dynamic efflux cycle is out of reach on the time scale of atomistic molecular dynamics simulations.

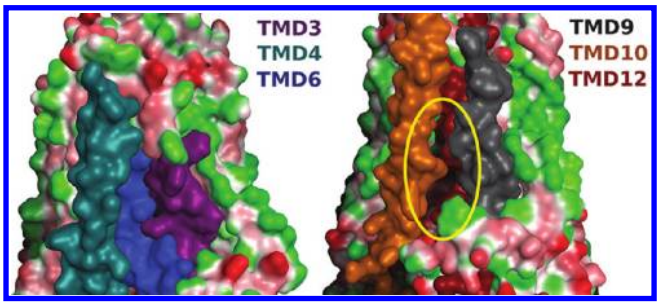

Figure 3. Surface representations of portals 4/6 closed (left) and 10/12 open (right). The channel is identified by the yellow oval curve, and the remaining structure is represented according to the lipophilicity (red, hydrophilic; green, hydrophobic).

Ligand–Protein Pocket Interactions. Molecules like verapamil, tariquidar, or latilagascene E can modulate the P-gp efflux cycle at a given point, not allowing the entrance of substrates or compromising the conformational changes required for the efflux process to take place.

Previous studies suggest that this modulation occurs due to a competitive inhibition with substrates for the drug-binding site,[93] enhanced by a high permeation rate within the lipid bilayer.[12,15] However, many of the substrates also have high log *P* values that favor the permeation within the membrane. Therefore, the difference between modulators and substrates can be due to the different number of interactions in the DBS.

In a previous work, the authors developed a pharmacophore[94] that identified hydrophobic and hydrogen-bond acceptor groups as responsible for the major interactions established within the drug-binding site. Previous studies also stated the importance of hydrophobic and hydrogen bond acceptor groups, correlating a large number of such moieties with a high affinity toward the structure.[95−97]

Table 1 presents the differences registered between the substrates and modulators. With the exception of QZ59-SSS, all modulators exhibit a higher number of nonbonded interactions, ranging from 1.1 to 2.3 when compared with substrates. These nonbonded interactions are with aromatic residues, as shown by the residue type more often involved in the modulator protein (except QZ59-SSS). Regarding the number of interactions, it is also shown that modulators frequently establish a higher number of simultaneous interactions. In the particular case of QZ59-SSS, with a more rigid scaffold, conformational changes that could increase the contact between the molecule and the residues in DBP are reduced, compromising this way the number of interactions established. The above data suggest that aromatic/hydrophobic contacts could be the key feature that determines the binding affinity for substrates/modulators within the DBP.

The ligand−P-gp interactions were studied and occurred extensively with TMD1, 3, 6, 11, and 12 but also in a smaller amount with TMD2, 5, 7, and 10 (Scheme S2 in the Supporting Information). This information is in accordance with a recent docking study which showed that main interactions occur with TMD5 and TMD6 but also with TMD1, TMD2, and TMD11.[39] Nevertheless, our study identified several residues and at least two regions where interactions occur exclusively with modulators (Scheme S2 in the Supporting Information). The first region is located at the beginning of TMD6, comprising residues Leu328, Thr329, Phe332, Ser333, and Leu335, and corresponds to an intersection of the QZ59-RRR and QZ59-SSS sites defined by Aller et al.[22] The other region includes residues from TMD7 (Ser725, Phe728), TMD10 (Glu871, Met874, Leu875), and TMD11 (Phe934). Several other residues were also identified to interact with at least three modulators and not with substrates (Met68, Phe332, Leu335, and Tyr946). In the particular case of tariquidar, a large number of residues are common to vinblastine and colchicine, which can

Table 1. Relative Average of Type and Number of Interactions and Residues (Relative to Substrates Vinblastine and Colchicine)[a]

	type of interaction		number of interactions			type of residues			
	hydrogen-bond interactions	nonbonded interactions	≤ 10 interactions	11−20 interactions	> 20 interactions	aromatic	aliphatic	polar	number of residues
VER/VIN	0.8	1.4	0.2	0.6	8.2	1.3	0.8	0.3	0.7
TAQ/VIN	1.3	1.1	0.6	1.0	2.8	1.5	1.3	1.1	1.3
LAG/VIN	0.2	1.2	1.0	0.9	2.4	1.0	0.8	0.7	0.8
QZS/VIN	0.2	0.8	2.6	0.6	0.2	0.7	0.7	0.4	0.6
VER/COL	1.4	2.3	0.1	1.4	41.0	2.0	1.1	0.8	1.2
TAQ/COL	2.2	1.6	0.2	2.2	14.0	2.3	1.9	3.3	2.3
LAG/COL	0.3	1.7	0.3	1.9	12.0	1.5	1.1	2.0	1.4
QZS/COL	0.4	1.2	0.8	1.3	1.0	1.0	1.0	1.3	1.1

[a]VER, verapamil; VIN, vinblastine; TAQ, tariquidar; LAG, latilagascene E; QZS, QZ59-SSS; COL, colchicine.

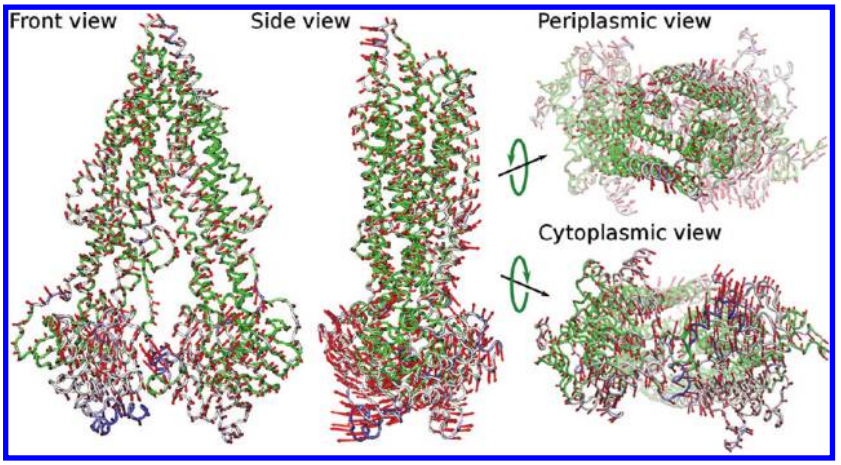

Figure 4. Normal motion patterns displayed by the *apo* P-gp.

suggest a possible competition for these residues. However, in TMD10/11, tariquidar establishes additional interactions with Met874, Leu875, and Phe934, not observed for any of the substrates, which could be correlated with the increased modulatory effect.

Another study, using docking over a homology model, also obtained similar results regarding the position of the molecules inside the drug binding pocket.[98] Interestingly, and despite the presence of other residues with hydrogen bond donor capabilities (as asparagine, serine, threonine, or tyrosine), throughout all simulations 65% of all hydrogen bonds within the DBP are registered with glutamine residues, particularly Gln721 and Gln942 (possibly due to the longer side-chain of this amino acid). The data obtained in the present study seem to support the hypothesis that the major differences between substrates and inhibitors resides in the number of interactions established with the DBP, this being the major driving force that eventually controls the efflux of the molecule.

Motion Pattern Analysis. P-Glycoprotein is an ATP-dependent efflux pump. Several studies describe the essential mechanism of action intimately related with the NBD dimerization after drug and nucleotide binding,[10] and helix rotation with consequent reduction of the DBS affinity,[33,97] TMD6 and TMD12 being intimately related with the translocation mechanism.[23,29]

The analysis of the motions in the 100 ns simulation (POPC-II) allowed the identification of the principal motion pattern for the transporter in the absence of a substrate (Figure 4). In this motion, the NBD2 has a pendular motion perpendicular to the bilayer plane, coupled with the NBD1 rotation around the longest molecular axis (perpendicular to the membrane plane). The linker seems to act as a damper in order to absorb stronger movements, therefore reducing the NBD fluctuations (Chart 1). This particular type of movement does not perturb the packing of the transmembranar helices, with no rotation of the TMD that could be linked to the efflux mechanism being observed.

The only distinct modification in the TMD was in TMD6, performing a "leverage-type" coordinated motion with TMD3 and TMD4 that allowed a more efficient adjustment of the transmembrane domains to the NBD motion patterns. This particular motion pattern of TMD6 is in agreement with a previously described pattern for Sav1866,[37] in which highly correlated motions between TMD6 and TMD3/4 were identified. However, for TMD12 (also implicated in the translocation mechanism), no coordinated motions were found. Therefore, our data suggest that TMD6 and TMD12 can be involved in two distinct roles of the efflux mechanism. While TMD12 could allow the access to the internal DBP through the formation of a channel with TMD10, TMD6 participates in motion patterns that can assist the propagation of conformational alterations.

As a way to unveil the presence of other motions linked to less intense eigenvectors but directly associated with the translocation mechanism, the volume of the internal cavity was calculated throughout the 100 ns simulation. A previous study[22] identified an internal cavity of approximately 6.0 nm^3. However, in our study, the initial cavity volume in the crystallographic structure after linker insertion was approximately 7.5 nm^3, a value which decreased to around 4 nm^3 (Chart 5), mainly due to a better helix repacking rather than shifts in the relative position of the linker upper loop.

Chart 5. Variation of the DBP Volume for the P-gp apo Structure

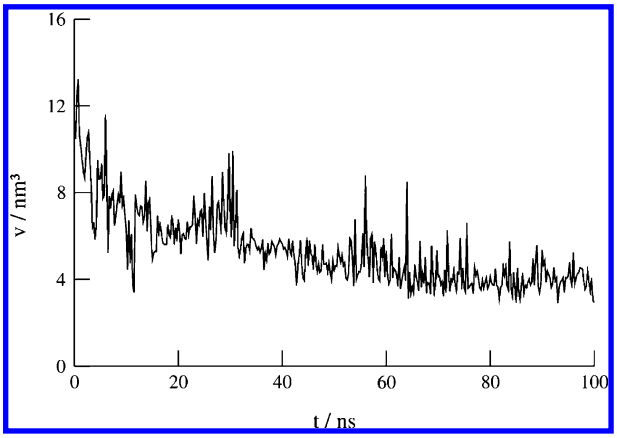

These differences in volume can be related, on one hand, with the lack of a lipid bilayer during the crystallization process (which allowed an expansion of the internal compartment) and, on the other, to the absence of the linker sequence in the crystallographic data, not permitting an exact definition of the DBP boundary. The changes in the DBP volume can be correlated with distinct motion patterns of P-gp. This fact is revealed by a more accurate analysis of the first 20 motion eigenvectors, from which it is possible to detect eigenvectors

3, 4, 10, and 15 as contributing to the motions associated with variations in the internal cavity volume.

Functional mode analysis (FMA) reveals that eigenvectors 3 and 4 are simple variations of the main oscillatory motion characterized by vectors 1 to 5. However, vectors 10 and 15 can be associated with a change in the distance between the NBDs and with helix rotation motions around the main P-gp molecular axis, leading to a contraction/expansion of the internal cavity, but to a very small degree. However, these vectors show that with the decrease of the distance between NBD1 and NBD2, the transmembranar domains tend to adjust through a clockwise rotation about the long molecular axis, leading to an expansion of the internal cavity.

To our knowledge, and corroborating previous studies in other transporters that relate the NBD dimerization with TMD conformational alterations to be important in the changes of the DBS-ligand affinity,[33,100,101] this is the first time that the existence of such motions in this transporter class have been shown in detail.

Another striking difference occurs when a molecule is placed inside the gate that allows access to the internal cavity. Vinblastine, a known substrate for P-gp, was placed directly in the "entrance gate" between TMD 10/12, and at a time interval of 20 ns, the motion patterns change substantially from normal oscillatory motions (linked with the *apo* structure as shown previously) into efflux-characteristic motions, with TMD helix rotations and NBD1-NBD2 distance fluctuations (Figure 5), similar to the motions found for vectors 10 and 15 in the *apo* structure. The main difference is that the efflux-characteristic motions are now observed in vector 1, the most dominant motion pattern. Additionally, the distance between NBD2 and the connecting loop between TMD8 and TMD9 tends to decrease (Figure 6), creating a pocket-like structure containing the residues directly involved in ATP binding. This observation corroborates recent studies where the entrance of a molecule suitable for efflux induces NBD conformational changes that favor ATP binding,[10] alterations intimately related with TMD12.[23] In addition, this conformational change in the NBD due to substrate binding can be a possible explanation for the initial step in the mechanism proposed by Siarhyeva et al.,[102] from which an ATP molecule in one NBD changes

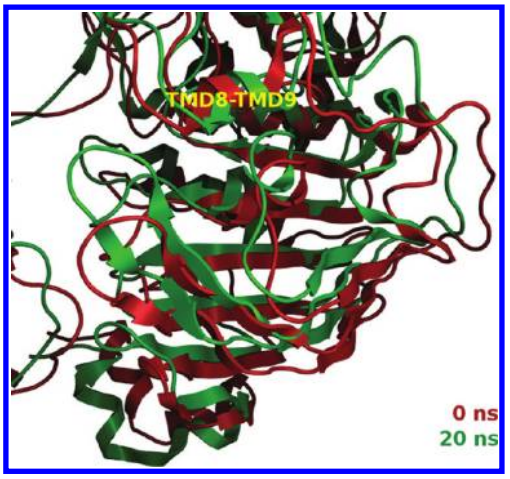

Figure 6. Conformation alterations at the ATP binding site after 20 ns (green) seen in the P-gp structure containing vinblastine at the "entrance gate" of the DBP.

from a "loose" to a "tight" state with consequent hydrolysis in the respective NBD. In fact, and based on several studies that described the interaction of a substrate as the initial point of the efflux cycle,[10,11] this signal produced by the substrate at the gate can produce conformational alterations, resulting in an approximation between the two NBD structures, allowing a more efficient binding of the ATP molecule[102] and initiating the catalytic cycle that expels molecules to the extracellular space. The evolution of the conformational changes also registers modifications in the vicinity of the vinblastine molecule and in both nucleotide binding domains, more specifically through the increase of the contact area. This fact is consistent with a recent study in the ABC hemolysin transporter that revealed alterations in the NBD contact areas after ATP hydrolysis.[36]

It was also found that the increase in contact area between the two NBDs creates an outward movement in TMD9, widening the TMD10/12 channel. Moreover, the formation of stable hydrogen bonds between vinblastine-asparagine residues 835/838 on TMD9 seems to induce a shift in the helix relative position that could possibly lead to the molecule internalization. However, in the absence of ATP, the volume variations

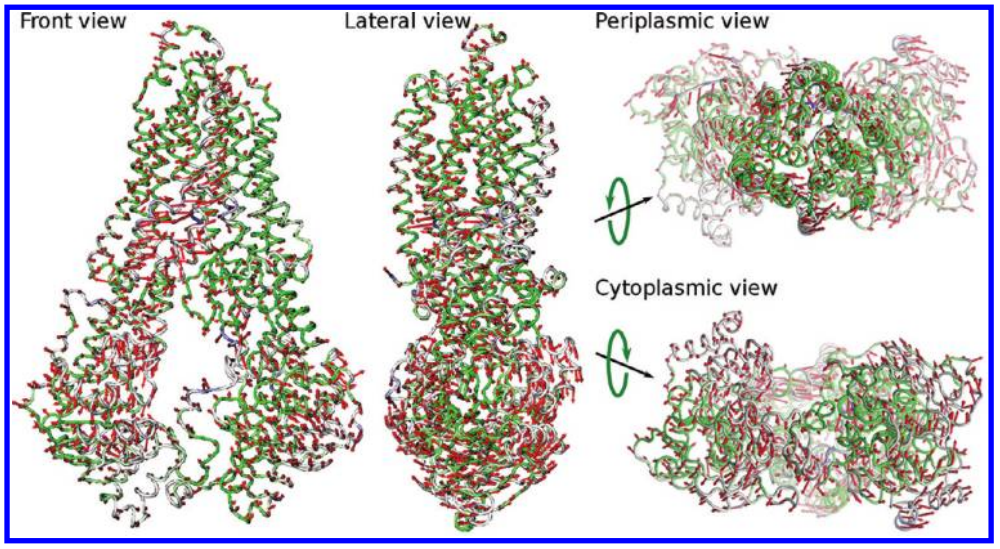

Figure 5. P-gp motion patterns associated with drug entrance through portal 10/12.

Chart 6. Variation in the Internal Cavity Volume after Vinblastine Docking

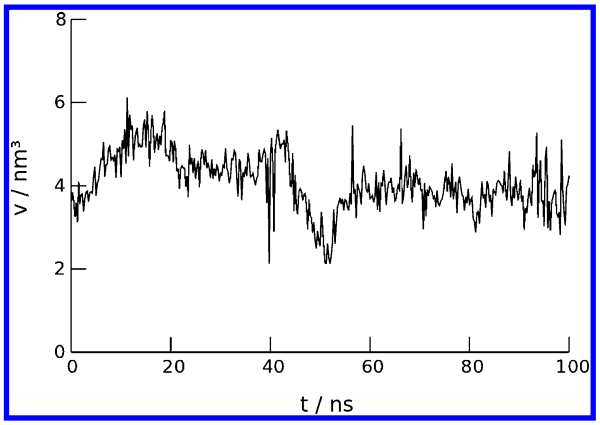

that occur are confined to a limited time interval, with the normal internal cavity volume restored after 60 ns (Chart 6).

CONCLUSION

In this study, the published crystallographic structure of murine P-glycoprotein was assessed in order to evaluate the structural stability through molecular dynamics simulations. To obtain a suitable structure for further studies like homology modeling, our investigation clarifies the importance of the lipid environment and missing linker in the transporter's stability. The present study shows that POPC is one of the most suitable lipids for this type of simulation and reveals that the missing linker segment displays a behavior similar to a damper, mediating the interactions between nucleotide-binding domains, thus contributing to an increase in the stability of the transporter. From the position acquired by the upper loop of the linker (near the inner leaflet interface), it can also be inferred that the access to the internal cavity becomes severely compromised, not validating the membranar pore model.

The present study also establishes substantial differences in the behavior of the DBP access portals previously identified. Whereas portal 4/6 remains closed throughout the simulations, not allowing access to the internal cavity, portal 10/12 remains open and accessible from the inner leaflet of the lipid bilayer but also from the intracellular membrane interface.

By means of covariance, normal and functional mode analysis, a "leverage-type" movement in TMD6 was identified that increases the stability of the remaining transmembranar domains. The same analysis identified motions that are currently accepted as the main driving force for the conformational changes during the efflux mechanism, namely the variation in the NBD distance (associated with NBD dimerization) and coordinated transmembranar helix rotations (with direct influence on the volume of the internal cavity). These motion patterns were also remarkably evident when a molecule (vinblastine) was docked in the 10/12 access portal. In only 20 ns, a strong modification was observed in the conformations of the TMD surrounding a vinblastine molecule (TMD 9, 10, and 12) with direct influence on the behavior of the NBD2 and in the motion patterns of the whole structure. All of the above facts are according to the hypothesis that the signal which triggers the efflux mechanism can be linked with the perturbation due to the presence and/or entrance into the internal cavity by a molecule suitable to efflux.

A molecular dynamics study with the 100 ns refined structure identified the number of interactions established between several ligands and DBP as a probable driven force that distinguishes inhibitors/modulators from substrates. This conclusion could be assessed through the analysis of the established protein–ligand interactions after 20 ns production runs in which several ligands were placed in three distinct locations of the DBP. The modulators studied consistently established a higher number of nonbonded interactions when compared with substrates (mainly aromatic), tariquidar being the modulator that interacted with a large number of different residues. In the particular case of verapamil, the classical gold-standard modulator in functional assays, it was been classified as a substrate since it is transported by P-gp. Previous studies demonstrated that the passive influx rate for this compound is higher when compared with classical substrates such as vinblastine, diffusing into the cell faster that P-gp can efflux, providing a way for competitive modulation.[12,16] Classical substrates do not show this type of behavior even at high concentrations. Considering the increased nonbonded interactions established in DBP by verapamil (also shown by modulators tariquidar and latilagascene E), this classifies the molecule as a modulator, in an intermediate level between substrates and inhibitors. In accordance with a previously developed pharmacophore,[94] the ability to establish a greater number of hydrophobic interactions within the pocket is one of the major features that allows a molecule to block competitively the substrate binding or to restrain conformational changes associated with the efflux mechanism.

We hope that this study may suggest new experimental ways to test the hypothesis that modulation is linked with interactions in specific regions and residues of the DBP described in this paper, aromatic interactions being one of the most relevant types. The mutation of residues in the sites proposed alone or in combination with chemical modification of the molecules can be two important experiments for validating this model. The chemical modifications should enhance or decrease activity due to the insertion or removal to a certain extent of aromatic moieties, respectively.

ASSOCIATED CONTENT

Supporting Information

A table listing the molecules included in this study and a scheme of the residue alignment for visual purposes. This material is available free of charge via the Internet at http://pubs.acs.org.

AUTHOR INFORMATION

Corresponding Author

*Tel.: +351 217946477. Fax: +351 217946470. E-mail: dsantos@ff.ul.pt.

Author Contributions

The manuscript was written through contributions of all authors.

Notes

The authors declare no competing financial interest.

ACKNOWLEDGMENTS

Financial support by Fundação para a Ciência e Tecnologia (FCT) is acknowledged through the research project PTDC/QUI-QUI/099815/2008 and PEst-OE/SAU/UI4013/2011.

ABBREVIATIONS

P-gp, P-glycoprotein; MDR, multidrug resistance; TMD, transmembranar domains; NBD, nucleotide-binding domains; ATP, adenosine triphosphate; DBS, drug-binding site; DBP, drug-binding pocket; DMPC, dimiristoylphosphatilylcholine; POPC, 1-palmitoyl-2-oleoyl-phospha-tidylcholine; MD, molecular dynamics; PBC, periodic boundary conditions; RMSD, root-mean-square deviation; RMSF, root-mean-square fluctuation

REFERENCES

(1) Juliano, R. L.; Ling, V. A surface glycoprotein modulating drug permeability in Chinese hamster ovary cell mutants. *Biochim. Biophys. Acta* **1976**, *455*, 152.

(2) Sharom, F. J. The P-glycoprotein Efflux Pump: How Does it Transport Drugs? *J. Membr. Biol.* **1997**, *160*, 161−175.

(3) Senior, A. E.; Al-Shawi, M. K.; Urbatsch, I. L. The catalytic cycle of P-glycoprotein. *FEBS Lett.* **1995**, *377*, 285−289.

(4) Borges-Walmsley, M. I.; McKeegan, K. S.; Walmsley, A. R. Structure and function of efflux pumps that confer resistance to drugs. *Biochem. J.* **2003**, *376*, 313−338.

(5) Altenberg, G. A.; Vanoye, C. G.; Horton, J. K.; Reuss, L.; Julie, K. Unidirectional fluxes of rhodamine 123 in multidrug-resistant cells: evidence against direct drug extrusion from the plasma membrane. *Proc. Natl. Acad. Sci. U. S. A.* **1994**, *91*, 4654−4657.

(6) Higgins, C. F.; Gottesman, M. M. Is the multidrug transporter a flippase? *Trends Biochem. Sci.* **1992**, *17*, 18−21.

(7) Raviv, Y.; Pollard, H. B.; Bruggemann, E. P.; Pastan, I.; Gottesman, M. M. Photosensitized labeling of a functional multidrug transporter in living drug-resistant tumor cells. *J. Biol. Chem.* **1990**, *265*, 3975−3980.

(8) Romsicki, Y.; Sharom, F. J. The membrane lipid environment modulates drug interactions with the P-glycoprotein multidrug transporter. *Biochemistry* **1999**, *38*, 6887−6896.

(9) Jones, P. M.; George, A. M. Opening of the ADP-bound active site in the ABC transporter ATPase dimer: Evidence for a constant contact, alternating sites model for the catalytic cycle. *Proteins* **2009**, *75*, 387−396.

(10) Callaghan, R.; Ford, R. C.; Kerr, I. D. The translocation mechanism of P-glycoprotein. *FEBS Lett.* **2006**, *580*, 1056−1063.

(11) Martin, C.; Berridge, G.; Mistry, P.; Higgins, C.; Charlton, P.; Callaghan, R. Drug Binding Sites on P-Glycoprotein Are Altered by ATP Binding Prior to Nucleotide Hydrolysis. *Biochemistry* **2000**, *39*, 11901−11906.

(12) Eytan, G. D.; Regev, R.; Oren, G.; Assaraf, Y. G. The role of passive transbilayer drug movement in multidrug resistance and its modulation. *J. Biol. Chem.* **1995**, *271*, 12897−12902.

(13) Urbatsch, I. L.; Senior, A. E. Effects of lipids on ATPase activity of purified Chinese hamster P-glycoprotein. *Arch. Biochem. Biophys.* **1995**, *316*, 135−140.

(14) Orlowski, S.; Martin, S.; Escargueil, A. P-glycoprotein and 'lipid rafts': some ambiguous mutual relationships (floating on them, building them or meeting them by chance?). *Cell. Mol. Life Sci.* **2006**, *63*, 1038−1059.

(15) Eytan, G.; Kuchel, P. Mechanism of Action of P-Glycoprotein in Relation to Passive Membrane Permeation. *Int. Rev. Cytol.* **1999**, *190*, 175−250.

(16) Regev, R.; Katzir, H.; Yeheskely-Hayon, D.; Eytan, G. D. Modulation of P-glycoprotein-mediated multidrug resistance by acceleration of passive drug permeation across the plasma membrane. *FEBS Lett.* **2007**, *274*, 6204−6214.

(17) Lee, A. G. Lipid−protein interactions in biological membranes: a structural perspective. *Biochim. Biophys. Acta* **2003**, *1612*, 1−40.

(18) Klappe, K.; Hummel, I.; Hoekstra, D.; Kok, J. W. Lipid dependence of ABC transporter localization and function. *Chem. Phys. Lipids.* **2009**, *161*, 57−64.

(19) Locher, K. P.; Lee, A. T.; Rees, D. C. The *E. coli* BtuCD structure: A framework for ABC transporter architecture and mechanism. *Science* **2002**, *296*, 1091−1098.

(20) Berman, H. M.; Westbrook, J.; Feng, Z.; Gilliland, G.; Bhat, T. N.; Weissig, H.; Shindyalov, I. N.; Bourne, P. E. The Protein Data Bank. *Nucleic Acids Res.* **2000**, *28*, 235−242.

(21) Berman, H. M.; Battistuz, T.; Bhat, T. N.; Bluhm, W. F.; Bourne, P. E.; Burkhardt, K.; Feng, Z.; Gilliland, G. L.; Iype, L.; Jain, S.; Fagan, P.; Marvin, J.; Padilla, D.; Ravichandran, V.; Schneider, B.; Thanki, N.; Weissig, H.; Westbrook, J. D.; Zardecki, C. The Protein Data Bank. *Acta Crystallogr., Sect. D: Biol. Crystallogr.* **2002**, *58*, 899−907.

(22) Aller, S. G.; Yu, J.; Ward, A.; Weng, Y.; Chittaboina, S.; Zhuo, R.; Harrell, P. M.; Trinh, Y. T.; Zhang, Q.; Urbatsch, I. L.; Chang, G. Structure of P-glycoprotein reveals a molecular basis for poly-specific drug binding. *Science* **2009**, *323*, 1718−1722.

(23) Crowley, E.; O'Mara, M. L.; Reynolds, C.; Tieleman, D. P.; Storm, J.; Kerr, I. D.; Callaghan, R. Transmembrane helix 12 modulates progression of the ATP catalytic cycle in ABCB1. *Biochemistry* **2009**, *48*, 6249−6258.

(24) Rothnie, A.; Storm, J.; Campbell, J.; Linton, K. J.; Kerr, I. D.; Callaghan, R. The coupling mechanism of P-glycoprotein involves residue L339 in the sixth membrane spanning segment. *J. Biol. Chem.* **2004**, *279*, 34913−34990.

(25) Ecker, G. F.; Stockner, T.; Chiba, P. Computational models for prediction of interactions with ABC-transporters. *Drug Discovery Today* **2008**, *13*, 311−317.

(26) Dawson, R. J.; Locher, K. P. Structure of a bacterial multidrug ABC transporter. *Nature* **2006**, *443*, 180−185.

(27) O'Mara, M. L.; Tieleman, D. P. P-glycoprotein models of the apo and ATP-bound states based on homology with Sav1866 and MalK. *FEBS Lett.* **2007**, *581*, 4217−4222.

(28) Ward, A.; Reyes, C. L.; Yu, J.; Roth, C. B.; Chang, G. Flexibility in the ABC transporter MsbA: Alternating access with a twist. *Proc. Natl. Acad. Sci. U. S. A.* **2007**, *104*, 19005−19010.

(29) Crowley, E.; Callaghan, R. Multidrug efflux pumps: drug binding − gates or cavity? *FEBS J.* **2010**, *277*, 530−539.

(30) Chang, G. Retraction of "Structure of MsbA from Vibrio cholera: A Multidrug Resistance ABC Transporter Homolog in a Closed Conformation" [J. Mol. Biol. (2003) 330 419−430]. *J. Mol. Biol.* **2007**, *369*, 596.

(31) Dawson, R. J.; Locher, K. P. Structure of the multidrug ABC transporter Sav1866 from Staphylococcus aureus in complex with AMP-PNP. *FEBS Lett.* **2007**, *581*, 935−938.

(32) Dong, J.; Yang, G.; McHaourab, H. S. Structural basis of energy transduction in the transport cycle of MsbA. *Science* **2005**, *308*, 1023−1028.

(33) Rosenberg, M. F.; Velarde, G.; Ford, R. C.; Martin, C.; Berridge, G.; Kerr, I. D.; Callaghan, R.; Schmidlin, A.; Wooding, C.; Linton, K. J.; Higgins, C. F. Repacking of the transmembrane domains of P-glycoprotein during the transport ATPase cycle. *EMBO J.* **2001**, *20*, 5615−5625.

(34) Rosenberg, M. F.; Callaghan, R.; Modok, S.; Higgins, C. F.; Ford, R. C. Three-dimensional structure of P-glycoprotein: the transmembrane regions adopt an asymmetric configuration in the nucleotide-bound state. *J. Biol. Chem.* **2005**, *280*, 2857−2862.

(35) Oliveira, A. S.; Baptista, A. M.; Soares, C. M. Conformational changes induced by ATP-hydrolysis in an ABC transporter: a molecular dynamics study of the Sav1866 exporter. *Proteins* **2011**, *79*, 1977−1990.

(36) Damas, J. M.; Oliveira, A. S.; Baptista, A. M.; Soares, C. M. Structural consequences of ATP hydrolysis on the ABC transporter NBD dimer: Molecular dynamics studies of HlyB. *Protein Sci.* **2011**, *20*, 1220−1230.

(37) Becker, J.-P.; Depret, G.; Van Bambeke, F.; Tulkens, P. M.; Prévost, M.; Bambeke, F. V. Molecular models of human P-glycoprotein in two different catalytic states. *BMC Struct. Biol.* **2009**, *9*, 1−18.

(38) Dolghih, E.; Bryant, C.; Renslo, A. R.; Jacobson, M. P. Predicting binding to P-Glycoprotein by Flexible Receptor Docking. *PLoS Comput. Biol.* **2011**, *7*, e1002083 DOI: 10.1371/journal.pcbi.1002083.
(39) Jabeen, I.; Wetwitayaklung, P.; Klepsch, F.; Parveen, Z.; Chiba, P.; Ecker, G. F. Probing the stereoselectivity of P-glycoprotein-synthesis, biological activity and ligand docking studies of a set of enantiopure benzopyrano[3,4-b][1,4]oxazines. *Chem. Commun. (Camb.)* **2011**, *47*, 2586−2588.
(40) Tsuruo, T.; Lida, H.; Tsukagoshi, S.; Sakurai, Y. Overcoming of Vincristine Resistance in P388 Leukemia in Vivo and in Vitro through Enhanced Cytotoxicity of Vincristine and Vinblastine by Verapamil. *Cancer Res.* **1981**, *41*, 1967−1972.
(41) Mistry, P.; Stewart, A. J.; Dangerfield, W.; Okiji, S.; Liddle, C.; Bootle, D.; Plumb, J. a.; Templeton, D.; Charlton, P. In vitro and in vivo reversal of P-glycoprotein-mediated multidrug resistance by a novel potent modulator, XR9576. *Cancer Res.* **2001**, *61*, 749−758.
(42) Hrycyna, C. A.; Airan, L. E.; Germann, U. A.; Ambudkar, S. V.; Pastan, I.; Gottesman, M. M. Structural flexibility of the linker region of human P-glycoprotein permits ATP hydrolysis and drug transport. *Biochemistry* **1998**, *37*, 13660−13673.
(43) Sato, T.; Kodan, A.; Kimura, Y.; Ueda, K.; Nakatsu, T.; Kato, H. Functional role of the linker region in purified human P-glycoprotein. *FEBS J.* **2009**, *276*, 3504−3516.
(44) Scott, W. R. P.; Hunenberger, P. H.; Tironi, I. G.; Mark, A. E.; Billeter, S. R.; Fennen, J.; Torda, A. E.; Huber, T.; Kruger, P.; van Gunsteren, W. F. The GROMOS Biomolecular Simulation Program Package. *J. Phys. Chem. A* **1999**, *103*, 3596−3607.
(45) Bonvin, A. M.; Mark, A. E.; van Gunsteren, W. F. The GROMOS96 benchmarks for molecular simulation. *Comput. Phys. Commun.* **2000**, *128*, 550−557.
(46) Oostenbrink, C.; Villa, A.; Mark, A. E.; van Gunsteren, W. F. A biomolecular force field based on the free enthalpy of hydration and solvation: the GROMOS force-field parameter sets 53A5 and 53A6. *J. Comput. Chem.* **2004**, *25*, 1656−1676.
(47) Poger, D.; Mark, A. E. On the Validation of Molecular Dynamics Simulations of Saturated and cis-Monounsaturated Phosphatidylcholine Lipid Bilayers: A Comparison with Experiment. *J. Chem. Theory Comput.* **2010**, *6*, 325−336.
(48) Poger, D.; Van Gunsteren, W. F.; Mark, A. E. A new force field for simulating phosphatidylcholine bilayers. *J. Comput. Chem.* **2010**, *31*, 1117−1125.
(49) Berger, O.; Edholm, O.; Jahnig, F. Molecular Dynamics Simulations of a Fluid Bilayer of Dipalmitoylphosphatidylcholine at Full Hydration, Constant Pressure, and Constant Temperature. *Biophys. J.* **1997**, *72*, 2002−2013.
(50) Chiu, S.-W.; Clark, M. A.; Balaji, V.; Subramaniam, S.; Scott, H. L.; Jakobsson, E. Incorporation of Surface Tension into Molecular Dynamics Simulation of Interface: A Fluid Phase Lipid Bilayer Membrane. *Biophys. J.* **1995**, *69*, 1230−1245.
(51) Kukol, A. Lipid models for United-atom Molecular Dynamics Simulations of Proteins. *J. Chem. Theory Comput.* **2009**, *5*, 615−626.
(52) Chandrasekhar, I.; Kastenholz, M.; Lins, R. D.; Oostenbrink, C.; Schuler, L. D.; Tieleman, D. P.; van Gunsteren, W. F. A consistent potential energy parameter set for lipids: dipalmitoylphospha-tidylcholine as a benchmark of the GROMOS96 45A3 force field. *Eur. Biophys. J.* **2003**, *32*, 67−77.
(53) Chandrasekhar, I.; Oostenbrink, C.; van Gunsteren, W. F. Simulating the physiological phase of hydrated DPPC bilayers: The Ester Moiety. *Soft Mater.* **2004**, *2*, 27−45.
(54) *Molecular Operating Environment (MOE)*, 2009.10; Chemical Computing Group Inc.: Montreal, QC, Canada, 2010.
(55) Berendsen, H. GROMACS: A message-passing parallel molecular dynamics implementation. *Comput. Phys. Commun.* **1995**, *91*, 43−56.
(56) Lindahl, E.; Hess, B.; van der Spoel, D. GROMACS 3.0: a package for molecular simulation and trajectory analysis. *J. Mol. Model.* **2001**, *7*, 306−317.
(57) van der Spoel, D.; Lindahl, E.; Hess, B.; Groenhof, G.; Mark, A. E.; Berendsen, H. J. GROMACS: fast, flexible, and free. *J. Comput. Chem.* **2005**, *26*, 1701−1718.
(58) Kandt, C.; Ash, W. L.; Tieleman, D. P. Setting up and running molecular dynamics simulations of membrane proteins. *Methods* **2007**, *41*, 475−488.
(59) Wolf, M. G.; Hoefling, M.; Aponte-Santamaría, C.; Grubmüller, H.; Groenhof, G. g_membed: Efficient insertion of a membrane protein into an equilibrated lipid bilayer with minimal perturbation. *J. Comput. Chem.* **2010**, *31*, 2169−2174.
(60) Allen, W. J.; Lemkul, J. A.; Bevan, D. R. GridMAT-MD: a grid-based membrane analysis tool for use with molecular dynamics. *J. Comput. Chem.* **2009**, *30*, 1952−1958.
(61) Hub, J. S.; de Groot, B. L. Detection of functional modes in protein dynamics. *PLoS Comput. Biol.* **2009**, *5*, e1000480 DOI: 10.1371/journal.pcbi.1000480.
(62) Amadei, A.; Linssen, A. B.; Berendsen, H. J. Essential dynamics of proteins. *Proteins* **1993**, *17*, 412−425.
(63) Bakan, A.; Meireles, L. M.; Bahar, I. ProDy: protein dynamics inferred from theory and experiments. *Bioinformatics* **2011**, *27*, 1575−1577.
(64) Bahar, I.; Lezon, T. R.; Bakan, A.; Shrivastava, I. H. Normal mode analysis of biomolecular structures: functional mechanisms of membrane proteins. *Chem. Rev.* **2010**, *110*, 1463−1497.
(65) Schüttelkopf, A. W.; van Aalten, D. M. PRODRG: a tool for high-throughput crystallography of protein-ligand complexes. *Acta Crystallogr., Sect. D: Biol. Crystallogr.* **2004**, *60*, 1355−1363.
(66) Malde, A. K.; Zuo, L.; Breeze, M.; Stroet, M.; Poger, D.; Nair, P. C.; Oostenbrink, C.; Mark, A. E. An Automated force field Topology Builder (ATB) and repository: version 1.0. *J. Chem. Theory Comput.* **2011**, *7*, 4026−4037.
(67) Frisch, M. J.; Trucks, G. W.; Schlegel, H. B.; Scuseria, G. E.; Robb, M. A.; Cheeseman, J. R.; Montgomery, J. A., Jr.; Vreven, T.; Kudin, K. N.; Burant, J. C.; Millam, J. M.; Iyengar, S. S.; Tomasi, J.; Barone, V.; Mennucci, B.; Cossi, M.; Scalmani, G.; Rega, N.; Petersson, G. A.; Nakatsuji, H.; Hada, M.; Ehara, M.; Toyota, K.; Fukuda, R.; Hasegawa, J.; Ishida, M.; Nakajima, T.; Honda, Y.; Kitao, O.; Nakai, H.; Klene, M.; Li, X.; Knox, J. E.; Hratchian, H. P.; Cross, J. B.; Bakken, V.; Adamo, C.; Jaramillo, J.; Gomperts, R.; Stratmann, R. E.; Yazyev, O.; Austin, A. J.; Cammi, R.; Pomelli, C.; Ochterski, J. W.; Ayala, P. Y.; Morokuma, K.; Voth, G. A.; Salvador, P.; Dannenberg, J. J.; Zakrzewski, V. G.; Dapprich, S.; Daniels, A. D.; Strain, M. C.; Farkas, O.; Malick, D. K.; Rabuck, A. D.; Raghavachari, K.; Foresman, J. B.; Ortiz, J. V.; Cui, Q.; Baboul, A. G.; Clifford, S.; Cioslowski, J.; Stefanov, B. B.; Liu, G.; Liashenko, A.; Piskorz, P.; Komaromi, I.; Martin, R. L.; Fox, D. J.; Keith, T.; Al-Laham, M. A.; Peng, C. Y.; Nanayakkara, A.; Challacombe, M.; Gill, P. M. W.; Johnson, B.; Chen, W.; Wong, M. W.; Gonzalez, C.; Pople, J. A. *Gaussian 03*, revision D.01; Gaussian, Inc.: Pittsburg, PA, 2004.
(68) Humphrey, W.; Dalke, A.; Schulten, K. VMD - Visual Molecular Dynamics. *J. Mol. Graphics* **1996**, *14*, 33−38.
(69) Lomize, M. A.; Lomize, A. L.; Pogozheva, I. D.; Mosberg, H. I. OPM: orientations of proteins in membranes database. *Bioinformatics* **2006**, *22*, 623−625.
(70) Petersen, B.; Petersen, T. N.; Andersen, P.; Nielsen, M.; Lundegaard, C. A generic method for assignment of reliability scores applied to solvent accessibility predictions. *BMC Struct. Biol.* **2009**, *9*, 51.
(71) Raghava, G. P. S. APSSP2: A combination method for protein secondary structure prediction based on neural network and example based learning. *CASP5* **2002**, *A-132*.
(72) Ouali, M.; King, R. D. Cascaded multiple classifiers for secondary structure prediction. *Protein Sci.* **2000**, *9*, 1162−1176.
(73) Chou, P. Y.; Fasman, G. D. Prediction of protein conformation. *Biochemistry* **1974**, *13*, 222−245.
(74) Lovell, S. C.; Davis, I. W.; Arendall, W. B., III; de Bakker, P. I. W.; Word, J. M.; Prisant, M. G.; Richardson, J. S.; Richardson, D. C. Structure validation by Cα geometry: ϕ,ψ and Cβ deviation. *Proteins* **2003**, *50*, 437−450.

(75) Leekumjorn, S.; Sum, A. K. Molecular Characterization of Gel and Liquid-Crystalline Structures of Fully Hydrated POPC and POPE Bilayers. *J. Phys. Chem. B* **2007**, *111*, 6026−6033.
(76) Duarte, N.; Gyémánt, N.; Abreu, P. M.; Molnár, J.; Ferreira, M.-J. U. New macrocyclic lathyrane diterpenes, from Euphorbia lagascae, as inhibitors of multidrug resistance of tumour cells. *Planta Med.* **2006**, *72*, 162−168.
(77) Wallace, A. C.; Laskowski, R. A.; Thornton, J. M. LIGPLOT: a program to generate schematic diagrams of protein-ligand interactions. *Protein Eng.* **1995**, *8*, 127−134.
(78) McDonald, I. K.; Thornton, J. M. Satisfying hydrogen bonding potential in proteins. *J. Mol. Biol.* **1994**, *238*, 777−793.
(79) Bussi, G.; Donadio, D.; Parrinello, M. Canonical sampling through velocity rescaling. *J. Chem. Phys.* **2007**, *126*, 14101−14107.
(80) Hoover, W. Canonical dynamics: Equilibrium phase-space distributions. *Phys. Rev. A* **1985**, *31*, 1695−1697.
(81) Nosé, S.; Klein, M. L. Constant pressure molecular dynamics for molecular systems. *Mol. Phys.* **1983**, *50*, 1055−1076.
(82) Parrinello, M.; Rahman, A. Polymorphic transitions in single crystals: A new molecular dynamics method. *J. Appl. Phys.* **1981**, *52*, 7182−7190.
(83) Darden, T.; York, D.; Pedersen, L. Particle mesh Ewald: An N·log(N) method for Ewald sums in large systems. *J. Chem. Phys.* **1993**, *98*, 10089.
(84) Essmann, U.; Perera, L.; Berkowitz, M. L.; Darden, T.; Lee, H.; Pedersen, L. G. A smooth particle mesh Ewald method. *J. Chem. Phys.* **1995**, *103*, 8577−8593.
(85) Miyamoto, S.; Kollman, P. A. Settle: An analytical version of the SHAKE and RATTLE algorithm for rigid water models. *J. Comput. Chem.* **1992**, *13*, 952−962.
(86) Hess, B.; Bekker, H.; Berendsen, H. J. C.; Fraaije, J. G.; LINCS, A Linear Constraint Solver for Molecular Simulations. *J. Comput. Chem.* **1997**, *18*, 1463−1472.
(87) Duque, D.; Li, X.-jun; Katsov, K.; Schick, M. Molecular theory of hydrophobic mismatch between lipids and peptides. *J. Chem. Phys.* **2002**, *116*, 10478−10481.
(88) Sun, T.; Liu, M.; Chen, W.; Wang, C. Molecular dynamics simulation of the transmembrane subunit of BtuCD in the lipid bilayer. *Sci. China Life Sci.* **2010**, *53*, 620−630.
(89) Rost, B.; Yachdav, G.; Liu, J. The PredictProtein server. *Nucleic Acids Res.* **2004**, *32*, W321 DOI: 10.1093/nar/gkh377.
(90) Kleywegt, G. J. Validation of protein crystal structures. *Acta Crystallogr.* **2000**, *D56*, 249−265.
(91) Law, R. J.; Capener, C.; Baaden, M.; Bond, P. J.; Campbell, J.; Patargias, G.; Arinaminpathy, Y.; Sansom, M. S. P. Membrane protein structure quality in molecular dynamics simulation. *J. Mol. Graphics Model.* **2005**, *24*, 157−165.
(92) Loo, T. W.; Clarke, D. M. Recent progress in understanding the mechanism of P-glycoprotein-mediated drug efflux. *J. Membr. Biol.* **2005**, *206*, 173−185.
(93) Akiyama, S.; Cornwell, M. M.; Kuwano, M.; Pastan, I.; Gottesman, M. M. Most drugs that reverse multidrug resistance also inhibit photoaffinity labeling of P-glycoprotein by a vinblastine analog. *Mol. Pharmacol.* **1988**, *33*, 144−147.
(94) Ferreira, R. J.; dos Santos, D. J.; Ferreira, M.-J.; Guedes, R. C. Toward a better pharmacophore description of P-glycoprotein modulators, based on macrocyclic diterpenes from Euphorbia species. *J. Chem. Inf. Model* **2011**, *51*, 1315−1324.
(95) Wiese, M.; Pajeva, I. K. Structure-activity relationships of multidrug resistance reversers. *Curr. Med. Chem.* **2001**, *8*, 685−713.
(96) Pajeva, I. K.; Wiese, M. Structure-activity relationships of tariquidar analogs as multidrug resistance modulators. *AAPS J.* **2009**, *11*, 435−444.
(97) Ekins, S.; Kim, R. B.; Leake, B. F.; Dantzig, A. H.; Schuetz, E. G.; Lan, L.-B.; Yasuda, K.; Shepard, R. L.; Winter, M. A.; Schuetz, J. D.; Wikel, J. H.; Wrighton, S. A. Three-Dimensional Quantitative Structure-Activity Relationships of Inhibitors of P-Glycoprotein. *Mol. Pharmacol.* **2002**, *61*, 964−973.
(98) Becker, J. P.; van Bambeke, F.; Tulkens, P. M.; Prévost, M. Dynamics and structural changes induced by ATP binding in SAV1866, a bacterial ABC exporter. *J. Phys. Chem. B* **2010**, *114*, 15948−15957.
(99) Ramachandra, M.; Ambudkar, S. V.; Chen, D.; Hrycyna, C. A.; Dey, S.; Gottesman, M. M.; Pastan, I. Human P-Glycoprotein Exhibits Reduced Affinity for Substrates during a Catalytic Transition State. *Biochemistry* **1998**, *37*, 4693−5038.
(100) Gutmann, D. A. P.; Ward, A.; Urbatsch, I. L.; Chang, G.; van Veen, H. W. Understanding polyspecificity of multidrug ABC transporters: closing in on the gaps in ABCB1. *Trends Biochem. Sci.* **2010**, *35*, 36−42.
(101) Gyimesi, G.; Ramachandran, S.; Kota, P.; Dokholyan, N. V.; Sarkadi, B.; Hegedűs, T. ATP hydrolysis at one of the two sites in ABC transporters initiates transport related conformational transitions. *Biochim. Biophys. Acta* **2011**, *1808*, 2954−2964.
(102) Siarheyva, A.; Liu, R.; Sharom, F. Characterization of an asymmetric occluded state of P-glycoprotein with two bound nucleotides: implications for catalysis. *J. Biol. Chem.* **2010**, *285*, 7575−7586.